Karlsruhe Institute of Technology

Institute for Theoretical Particle Physics

Phenomenology of Flavoured Dark Matter in Dark Minimal Flavour Violation

KSETA Plenary Workshop, Durbach

Monika Blanke, **Simon Kast** | Feb 13, 2017

KARLSRUHE INSTITUTE OF TECHNOLOGY

Outline

Dark Matter Evidence

- 1933: Virial theorem $2T = -U$ applied to coma cluster.

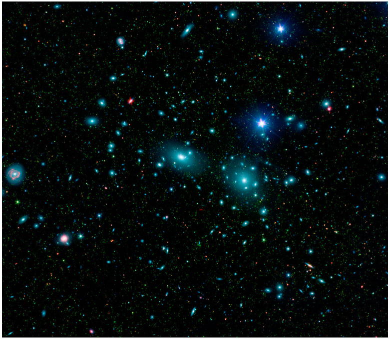

Figure : Coma cluster.

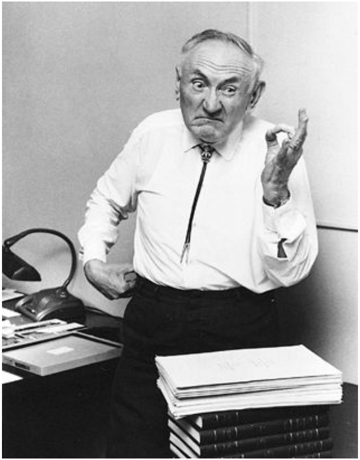

Figure : Fritz Zwicky.

Dark Matter Evidence

- 1970's: Rotation curves of stars in galaxies.

Figure : Vera Rubin.

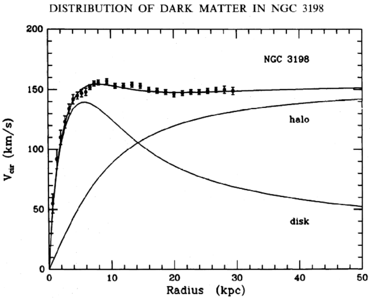

Figure : Rotation curve data vs. predictions.

Dark Matter Evidence

- After recombination baryonic structure formation profits from preexisting dense DM regions
  $\Rightarrow$ galaxy formation possible in age of the Universe.

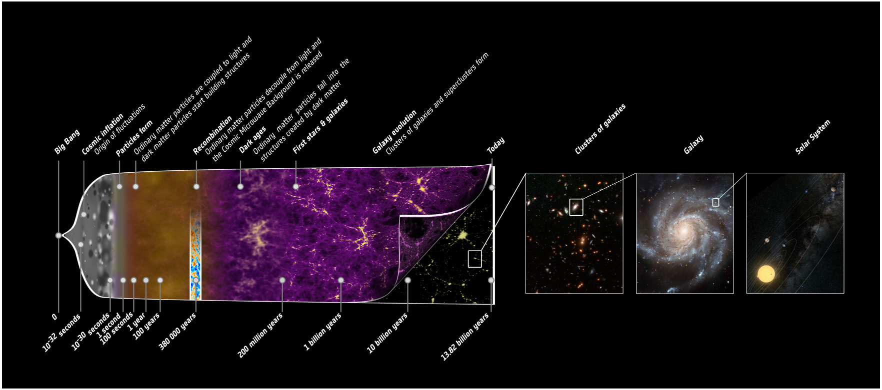

Figure : History of the Universe.

Dark Matter Evidence

- Gravitational lensing effects $\rightarrow$ Bullet Cluster. Misalignment of visible and gravitational mass distribution.

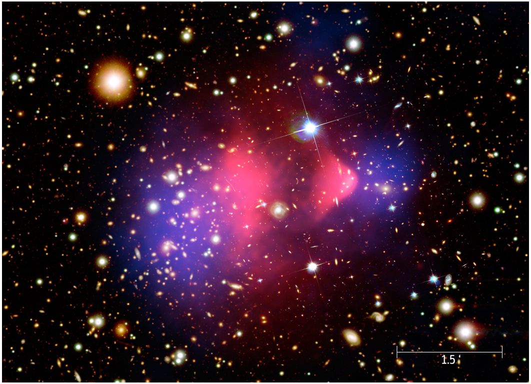

Figure : Bullet cluster. Visible matter distribution (red) and dark matter distribution (blue).

Dark Matter Evidence

- Imprints in Cosmic Microwave Background (CMB).

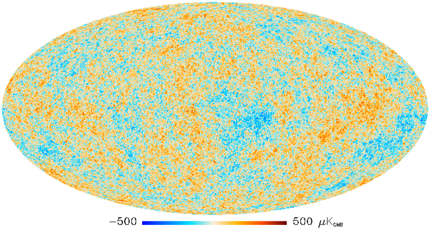

Figure : Temperature fluctuations in CMB (Planck 2013).

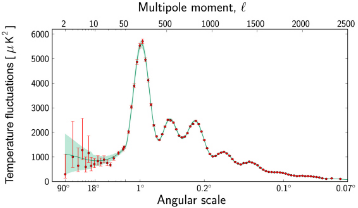

Figure : CMB power spectrum (Planck 2013).

Approaches to identify Dark Matter

- Extension of SM motivated by a new idea solving several problems (e.g. SUSY, Axions).
- Study of all kind of higher dimensional effective SM-DM interactions in Effective Field Theory (EFT).
- **Simplified models**: Study phenomenology of specific interactions with limited number of parameters.

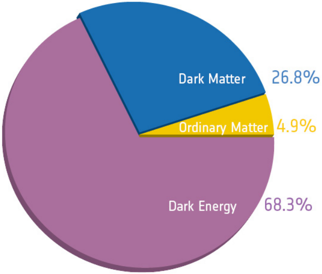

Figure : Energy distribution of the Universe (Planck 2015).

The Flavour Gate to Dark Matter

Assume an analogy to the SM fermions $\rightarrow$ dark flavour triplet $\begin{pmatrix} \chi_u \\ \chi_c \\ \chi_t \end{pmatrix}$.

The Flavour Gate to Dark Matter

Assume an analogy to the SM fermions $\rightarrow$ dark flavour triplet $\begin{pmatrix} \chi_u \\ \chi_c \\ \chi_t \end{pmatrix}$.

Flavoured Dark Matter coupling to SM right-handed up-quark triplet:

- DM flavour triplet χ_j, Dirac fermion, SM gauge singlet.
- Heavy scalar mediator ϕ, carrying colour and hypercharge.
- Lagrangian has unbroken $\mathbb{Z}_3$ symmetry and hence yields stability of DM χ (for $m_\phi > m_\chi$).

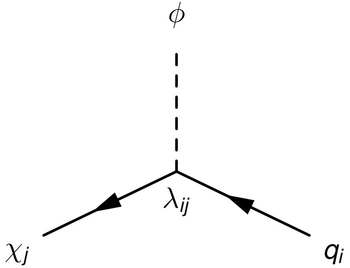

Figure : New physics interaction (basic vertex).

Dark Minimal Flavour Violation (DMFV)

Karlsruhe Institute of Technology

[Agrawal, Blanke, Gemmler '14]

Minimal Flavour Violation:

- Standard approach.
- Structure of λ_{ij} simple and completely determined by SM Yukawa couplings.
- Limited number of free parameters left in model.
- Easier to analyze limited phenomenology.

Dark Minimal Flavour Violation:

- Novel approach.
- Structure of λ_{ij} left general and as a new source of flavour and CP violating effects.
- Extended number of free parameters from coupling: 3 "couplings" $D_{\lambda,ii}$, 3 "mixing angles" θ_{ij}, 3 "phases" δ_{ij}.
- More complicated but also more interesting phenomenology.

How to Detect Flavoured Dark Matter?

KIT
Karlsruhe Institute of Technology

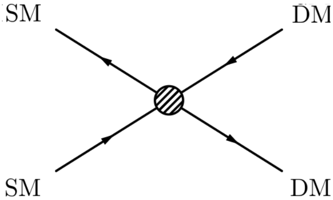

collider searches

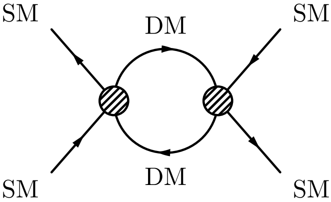

precision flavour data

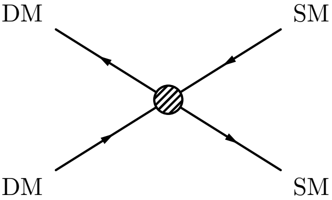

indirect detection / freeze-out

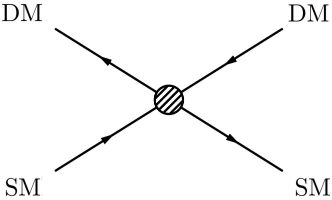

direct detection

Constraints from Colliders

- Study the process $pp \to \phi\phi^\dagger \to q\bar{q}\chi\bar{\chi}$.
- Depending on decay product of ϕ we detect either a top-signature or a jet ($+\not{E}_T$).
- Inspiration from SUSY searches at LHC [ATLAS collaboration '14].
  $\Rightarrow$ Upper bounds on CS of both $t\bar{t}$ and dijet signals.
- Those constraints translate to lower bound on mediator mass and upper bound on "couplings".

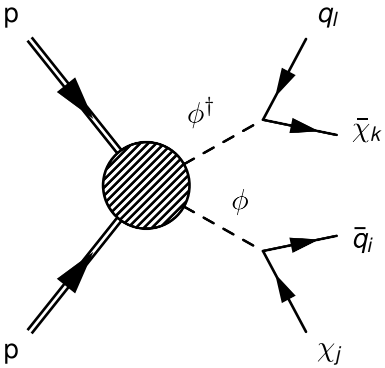

Figure : Studied LHC DM production processes.

Constraints from Flavour Precision Data

- No mesons with top-quark are possible, the only constraints come from D-mesons.
  $\Rightarrow$ not too strong
- The NP contribution has to be smaller than experimental bounds [UTfit collaboration '14].
- Mixing angles are associated with CP violation phases.
  $\Rightarrow$ get constrained

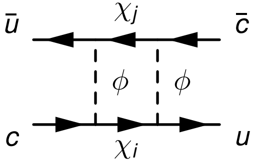

Figure : NP contr. to neutral D-meson mixing.

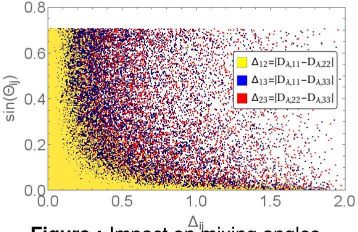

Figure : Impact on mixing angles.

DM Constraints from Observed Relic Abundance

- Assume DM abundance as a thermal relic.
  $\Rightarrow$ SM matter and DM used to be in thermal equilibrium in early universe.
  $\Rightarrow$ Same order of magnitude for energy content.

- Freeze-out: annihilation rate VS expansion.
  $\Rightarrow$ Remaining relic DM depends on speed of annihilation, i.e. on the cross section

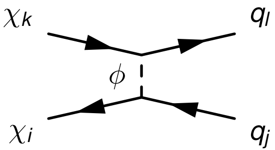

Figure : Annihilation of DM flavours.

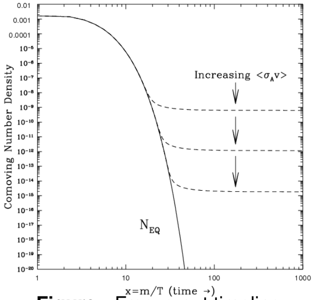

Figure : Freeze-out timeline.

DM Constraints from Observed Relic Abundance

- Annihilation cross section needs to have just the right value (in tolerance interval) [Steigman, Dasgupta, Beacom '12] to produce the observed relic DM.

$$\langle \sigma v \rangle_{eff} \approx\approx\approx \lambda^4 \frac{m_\chi^2}{m_\phi^4}$$

DM Constraints from Observed Relic Abundance

- Annihilation cross section needs to have just the right value (in tolerance interval) [Steigman, Dasgupta, Beacom '12] to produce the observed relic DM.

$$\langle \sigma v \rangle_{eff} \approx\approx\approx \lambda^4 \frac{m_\chi^2}{m_\phi^4}$$

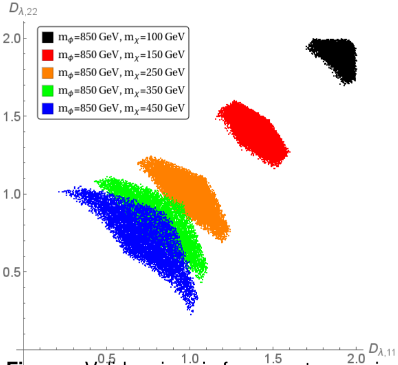

Figure : Valid regions in freeze-out scenario.

DM Constraints from Observed Relic Abundance

- Annihilation cross section needs to have just the right value (in tolerance interval) [Steigman, Dasgupta, Beacom '12] to produce the observed relic DM.

$$\langle \sigma v \rangle_{eff} \approx\approx\approx \lambda^4 \frac{m_\chi^2}{m_\phi^4}$$

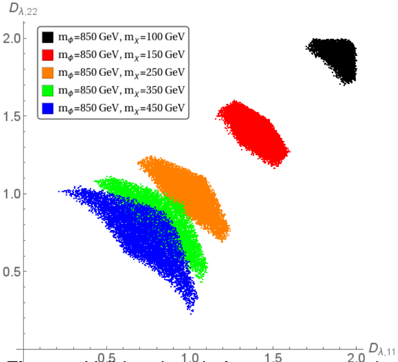

Figure : Valid regions in freeze-out scenario.

- Actual form of CS more complicated and dependent on several criteria.

Constraints from Direct Detection Experiments

- Foremost liquid Xenon experiments.
- Current best bounds from LUX data [LUX collaboration '16].
- Several future experiments in pursuit.

Figure : Xenon chamber of LUX experiment.

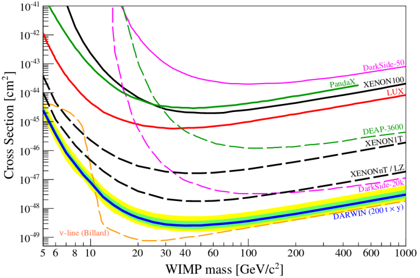

Figure : Bounds of current and future direct detection experiments.

Constraints from Direct Detection Experiments

Many contributions to total WIMP-nucleon cross section:

$$\sigma_n^{SI} = \frac{\mu_n^2}{\pi A^2} |Zf_p + (A - Z) f_n|^2.$$

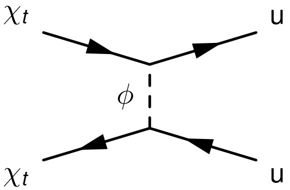

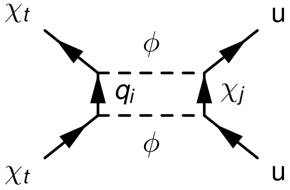

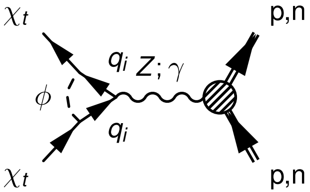

Constraints from Direct Detection Experiments

Figure : Cancellation of tree-level and neutron Z-penguin contributions (symbolic).

- Cancellation forces mixing angle.
- Xenon has several stable isotopes.

  $\Rightarrow$ Simultaneous suppression.
- Future bounds exclude high couplings.

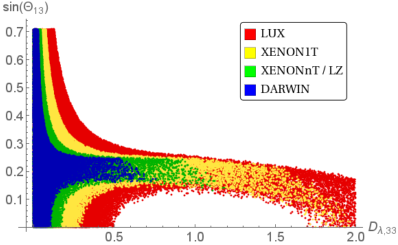

Figure : Valid mixing angle vs coupling.

Results of Combined Analysis

- Interplay of different constraints.
- For given m_χ and m_ϕ relic abundance constraints will determine coupling strength.
- Upper bound of possible coupling strength from direct detection constraints

$\Rightarrow$ Lower bound on DM mass from the combination (in dependence of mediator mass)

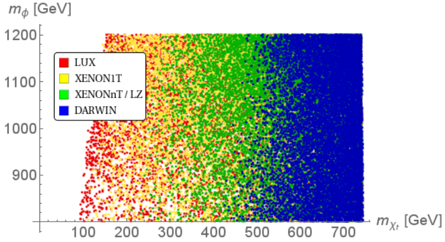

Figure : Valid regions for different strengths of direct detection constraints.

Results of Combined Analysis

- Interplay of different constraints.
- For given m_χ and m_ϕ relic abundance constraints will determine coupling strength.
- Upper bound of possible coupling strength from direct detection constraints

$\Rightarrow$ Lower bound on DM mass from the combination (in dependence of mediator mass)

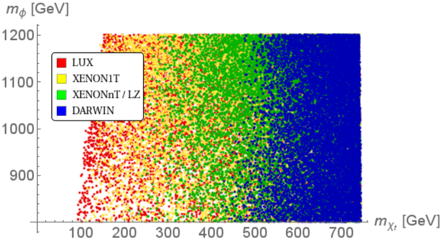

Figure : Valid regions for different strengths of direct detection constraints.

Many more interesting details and other effects.

Summary and Outlook

- Simplified model of flavoured dark matter.
- Leave coupling general (Dark Minimal Flavour Violation).
- Demanding phenomenologically interesting DM mass in combination with constraints also has impact on other parameters.
- Interesting interplay of constraints.
- Future direct detection experiments have large impact on parameter-space.

The End

Thank you!

The End

Karlsruhe Institute of Technology

Thank you!

Questions?

References I

- Georges Aad et al. "Search for squarks and gluinos with the ATLAS detector in final states with jets and missing transverse momentum using $\sqrt{s} = 8$ TeV proton–proton collision data". In: *JHEP* 09 (2014), p. 176. DOI: 10.1007/JHEP09(2014)176. arXiv: 1405.7875 [hep-ex].
- Georges Aad et al. "Search for top squark pair production in final states with one isolated lepton, jets, and missing transverse momentum in $\sqrt{s}$ =8 TeV *pp* collisions with the ATLAS detector". In: *JHEP* 11 (2014), p. 118. DOI: 10.1007/JHEP11(2014)118. arXiv: 1407.0583 [hep-ex].
- R Aaij et al. "Precision measurement of D meson mass differences". In: *JHEP* 1306 (2013), p. 065. DOI: 10.1007/JHEP06(2013)065. arXiv: 1304.6865 [hep-ex].

References II

- Prateek Agrawal, Monika Blanke, and Katrin Gemmler. "Flavored dark matter beyond Minimal Flavor Violation". In: *JHEP* 1410 (2014), p. 72. DOI: 10.1007/JHEP10(2014)072. arXiv: 1405.6709 [hep-ph].
- D. S. Akerib et al. "Improved WIMP scattering limits from the LUX experiment". In: (2015). arXiv: 1512.03506 [astro-ph.CO].
- Sinya Aoki et al. "Review of lattice results concerning low-energy particle physics". In: *Eur.Phys.J.* C74 (2014), p. 2890. DOI: 10.1140/epjc/s10052-014-2890-7. arXiv: 1310.8555 [hep-lat].
- A.J. Bevan et al. "The UTfit collaboration average of D meson mixing data: Winter 2014". In: *JHEP* 1403 (2014), p. 123. DOI: 10.1007/JHEP03(2014)123. arXiv: 1402.1664 [hep-ph].

References III

- Monika Blanke et al. "FCNC Processes in the Littlest Higgs Model with T-Parity: a 2009 Look". In: *Acta Phys.Polon.* B41 (2010), pp. 657–683. arXiv: `0906.5454 [hep-ph]`.
- N. Carrasco et al. "$D^0-\bar{D}^0$ mixing in the standard model and beyond from N_f =2 twisted mass QCD". In: *Phys.Rev.* D90.1 (2014), p. 014502. DOI: `10.1103/PhysRevD.90.014502`. arXiv: `1403.7302 [hep-lat]`.
- Carlos A. Chavez, Ray F. Cowan, and W.S. Lockman. "Charm meson mixing: An experimental review". In: *Int.J.Mod.Phys.* A27 (2012), p. 1230019. DOI: `10.1142/S0217751X12300190`. arXiv: `1209.5806 [hep-ex]`.

References IV

Csaba Csaki, Adam Falkowski, and Andreas Weiler. “The Flavor of the Composite Pseudo-Goldstone Higgs”. In: *JHEP* 0809 (2008), p. 008. DOI: 10.1088/1126-6708/2008/09/008. arXiv: 0804.1954 [hep-ph].

Yuval Grossman, Yosef Nir, and Gilad Perez. “Testing New Indirect CP Violation”. In: *Phys.Rev.Lett.* 103 (2009), p. 071602. DOI: 10.1103/PhysRevLett.103.071602. arXiv: 0904.0305 [hep-ph].

Alexander L. Kagan and Michael D. Sokoloff. “On Indirect CP Violation and Implications for D0 - anti-D0 and B(s) - anti-B(s) mixing”. In: *Phys.Rev.* D80 (2009), p. 076008. DOI: 10.1103/PhysRevD.80.076008. arXiv: 0907.3917 [hep-ph].

References V

Can Kilic, Matthew D. Klimek, and Jiang-Hao Yu. “Signatures of Top Flavored Dark Matter”. In: *Phys.Rev.* D91.5 (2015), p. 054036. DOI: 10.1103/PhysRevD.91.054036. arXiv: 1501.02202 [hep-ph].

Alexey A Petrov. “Long-distance effects in charm mixing”. In: (2013). arXiv: 1312.5304 [hep-ph].

Gary Steigman, Basudeb Dasgupta, and John F. Beacom. “Precise Relic WIMP Abundance and its Impact on Searches for Dark Matter Annihilation”. In: *Phys.Rev.* D86 (2012), p. 023506. DOI: 10.1103/PhysRevD.86.023506. arXiv: 1204.3622 [hep-ph].

James D. Wells. “Annihilation cross-sections for relic densities in the low velocity limit”. In: (1994). arXiv: hep-ph/9404219 [hep-ph].

The Flavour Gate to Dark Matter

[Agrawal, Blanke, Gemmler '14]

Assume an analogy to the SM fermions $\rightarrow$ dark flavour triplet χ_i.

The Flavour Gate to Dark Matter

[Agrawal, Blanke, Gemmler '14]

Assume an analogy to the SM fermions → dark flavour triplet χ_i.

Flavoured Dark Matter coupling to SM right-handed up-quark triplet:

$$\mathcal{L}_{\text{NP,int}} = -\lambda_{ij}\bar{u}_{Ri}\chi_j\phi + h.c.$$

$$\mathcal{L}_{\text{NP,mass}} = -m_\phi\phi^\dagger\phi - m_\chi\bar{\chi}\chi$$

- DM flavour triplet χ_j, Dirac fermion, SM gauge singlet.
- Heavy scalar mediator ϕ, carrying colour and hypercharge.
- Lagrangian has unbroken $\mathbb{Z}_3$ symmetry and hence yields stability of DM χ (for $m_\phi > m_\chi$).

Dark Minimal Flavour Violation

[Agrawal, Blanke, Gemmler '14]

Flavour Symmetry

$$U(3)_u \times U(3)_d \times U(3)_q \times U(3)_\chi$$

is only broken by SM Yukawa couplings and the DM-quark coupling λ_{ij} (Dark Minimal Flavour Violation).

$\Rightarrow$ Beyond Minimal Flavour Violation.

$\Rightarrow$ only DM mass splitting comes from RG running:

$$m_{ij} = m_\chi(\mathbb{1} + \eta\lambda^\dagger\lambda + ...)_{ij} = m_\chi(1 + \eta(D_{\lambda,ii})^2 + ...)\delta_{ij}.$$

- η depends on the full theory $\rightarrow$ has to be a parameter of the simplified model.
- flavour with lowest mass is our DM candidate.
  $\rightarrow$ we choose the "top-flavour". [Kilic, Klimek, Yu '15]

Parametrization of DM-Quark Coupling Matrix

Dark Minimal Flavour Violation (DMFV): λ_{ij} is a general 3×3 coupling matrix $\rightarrow$ 9 real parameters and 9 complex phases.

- Can be split up as (bilinear diagonalization):

$$\lambda = U^{\lambda} D_{\lambda} V^{\lambda}$$

  with unitary matrices U^{λ}, V^{λ} and diagonal real matrix D_{λ}.
- Use redundancy to eliminate 3 phases in U^{λ}.
- Use flavour symmetry in dark sector $U(3)_{\chi}$ to get rid of V^{λ}

After using all the symmetries at our disposal λ has 9 parameters left and can be parametrized as:

$$\lambda = U_{23}^{\lambda} U_{13}^{\lambda} U_{12}^{\lambda} D_{\lambda}$$

Constraints from SUSY Searches at LHC

[ATLAS collaboration '14]

- Study the process $pp \to \phi\phi^\dagger \to q\bar{q}\chi\bar{\chi}$.
- Depending on decay product of ϕ we detect either a top-signature or a jet ($+\not{E}_T$).
- Inspiration from SUSY searches at LHC
  $\Rightarrow$ Upper bounds on CS of both $t\bar{t}$ and dijet signals.

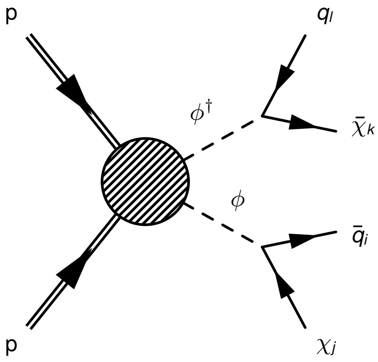

Figure : Studied LHC DM production processes.

Constraints from SUSY Searches at LHC

Involved QCD processes

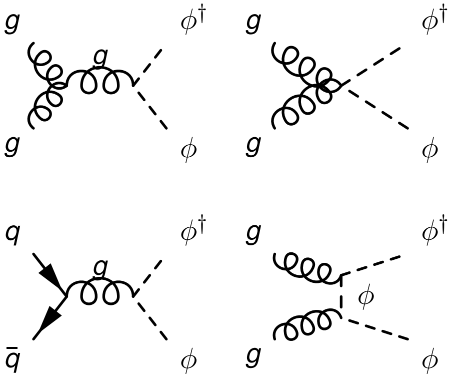

Involved NP processes

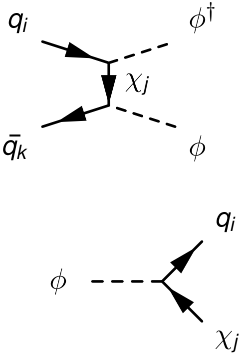

References

Constraints from $t\bar{t}+\not{E}_T$ Searches at LHC

- $D_{\lambda,33}$ increased
  $\rightarrow$ BR of decay goes up.
- $D_{\lambda,11}$, $D_{\lambda,22}$ increased
  $\rightarrow$ BR of decay goes down.

- **BUT**: For high $D_{\lambda,11} = D_{\lambda,22}$ we observe increasing excluded areas.

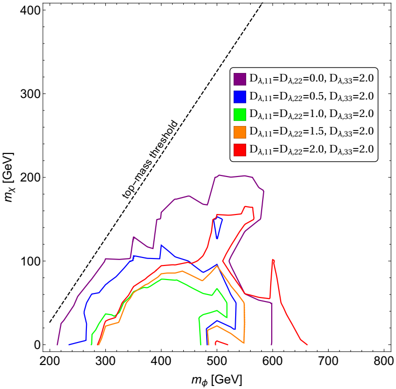

Figure : Exclusion plot for $t\bar{t}$ final state, mixing angles set to zero.

References

Constraints from SUSY Searches at LHC

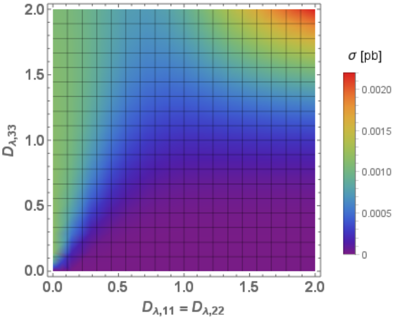

Figure : Cross section of $t\bar{t}$ final state for $m_\phi = 850$ GeV and $m_\chi = 50$ GeV, mixing angles set to zero.

Explanation: NP production

- Major contribution to total production (for high $D_{\lambda,11}$, $D_{\lambda,22}$)
- This effect can make up for drop in BR
- $D_{\lambda,33}$ not relevant, since the protons do not contain top
- Very high couplings can lead to serious exclusion areas.

References

Constraints from dijet + $\not{E}_T$ Searches at LHC

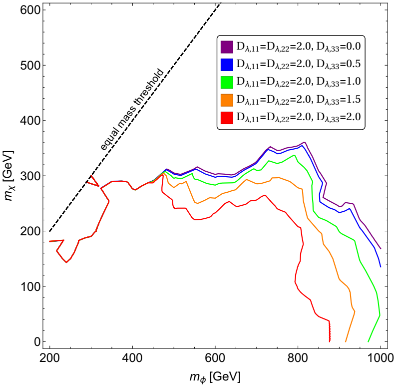

Figure : Exclusion plot for dijet final state, mixing angles set to zero.

- Stronger exclusion bounds on model.
- The phenomenologically interesting region is $m_\chi \leq 1$ TeV.
- Too large couplings $D_{\lambda,ii}$ would exclude nearly all of parameter space.
- Most serious constraints come from dijet final state.

$\Rightarrow$ Safe parameter-space:

$$m_\phi \geq 850 \text{ GeV}$$

$$2.0 \geq D_{\lambda,33} \geq D_{\lambda,22}, D_{\lambda,11}$$

Influence of Mixing Angles on LHC production

- Mixing angles shift influences between couplings $D_{\lambda,ii}$.
  $\Rightarrow$ For big splitting in the couplings, mixing angles can cause big shifts in cross sections.
- For our choice of m_ϕ bounds from $t\bar{t}$ final state cause no constraints.
- Worst allowed case for dijet final state, in our safe parameter-space, is $D_{\lambda,11} = D_{\lambda,22} = D_{\lambda,33} = 2.0$
  $\Rightarrow$ Unchanged by mixing angles.

$\Rightarrow$ Mixing angles can cause no problem with this choice of safe parameter-space.

Flavour Constraints from Neutral Meson Mixing

[UTfit collaboration '14]

- No mesons with top-quark are possible, the only constraints come from D-mesons.
  $\Rightarrow$ not too strong
- The NP contribution has to be smaller than experimental bounds.

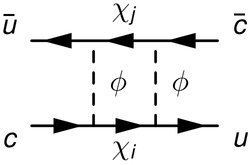

Figure : NP contr. to neutral D-meson mixing.

$$M_{12}^{D,NP} = \frac{1}{2m_D}\langle \bar{D}^0|\mathcal{H}_{eff}^{\Delta C=2,new}|D^0\rangle^* = \frac{1}{384\pi^2 m_\phi^2}\sum_{i,j}\lambda_{uj}^*\lambda_{cj}\lambda_{ui}^*\lambda_{ci}\cdot L(x_i,x_j)\cdot\eta_D\cdot m_D f_D^2\hat{B}_D.$$

References

Flavour Constraints from Neutral Meson Mixing

$$\left((\lambda\lambda^\dagger)_{cu}\right)^2 = \left((U_\lambda D_\lambda D_\lambda^\dagger U_\lambda^\dagger)_{cu}\right)^2$$

- For degeneracy $D_{\lambda,11} = D_{\lambda,22} = D_{\lambda,33}$ the mixing matrices U_{ij}^λ will drop out.
- The higher the splitting $\Delta_{ij} = D_{\lambda,ii} - D_{\lambda,jj}$, the more we will see the constraints on the mixing angle θ_{ij}.

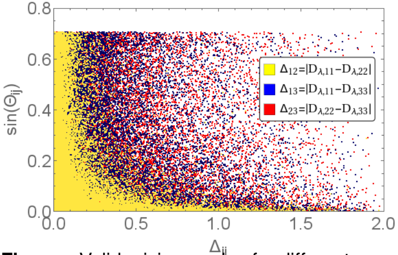

Figure : Valid mixing angles for different coupling splittings. $m_\phi = 850$ GeV and $m_\chi = 250$ GeV.

$\Rightarrow$ Most significant constraints on θ_{12}, other mixings nearly unconstrained.

DM Constraints from Observed Relic Abundance

[Steigman, Dasgupta, Beacom '12]

- Assume DM abundance as a thermal relic, $T_f \propto \frac{m_\chi}{20}$
- Annihilation CS has to be just large enough to produce the correct relic density (we allow for a 10% tolerance interval):

$$\langle \sigma v \rangle_{eff,exp} = 2.2 \times 10^{-26}\text{cm}^3/\text{s}.$$

$\Rightarrow$ cuts out valid area for $D_{\lambda,ii}$ depending on m_ϕ and m_χ

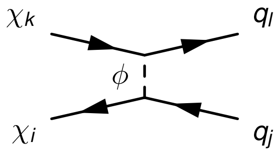

Figure : Annihilation of DM flavours.

$$\langle \sigma v \rangle_{eff} = \frac{1}{9} \times \frac{3}{256\pi} \sum_{i,j=1,2,3} \sum_{k,l=u,c,t} \lambda_{ki}\lambda_{ki}^*\lambda_{lj}\lambda_{lj}^* \frac{\sqrt{\left(4m_\chi^2 - (m_k - m_l)^2\right)\left(4m_\chi^2 - (m_k + m_l)^2\right)}}{\left(m_\phi^2 + m_\chi^2 - \frac{m_k^2}{2} - \frac{m_l^2}{2}\right)^2}.$$

DM Constraints from Observed Relic Abundance

- Depending on the mass splitting of the different DM flavours several freeze-out scenarios are possible.

$$m_{ij} = m_\chi(1 + \eta(D_{\lambda,ii})^2 + ...)\delta_{ij}.$$

- For a DM mass below the top-quark mass this decay channel drops out.

  $\Rightarrow$ CS formula and hence impact on parameters can be quite different

- Extreme example: only χ_t present at freeze-out with DM mass below top mass threshold:

$$\langle\sigma v\rangle_{eff} = \frac{3}{256\pi}\sum_{k,l=u,c}\lambda_{k3}\lambda^*_{k3}\lambda_{l3}\lambda^*_{l3}\frac{4m_\chi^2}{\left(m_\phi^2 + m_\chi^2\right)^2}.$$

Quasi-Degenerate Freeze-Out (QDF) Szenario

- All DM flavours are present at the freeze-out.
- We require the mass splitting to be less than 1% (significantly smaller than T_f) for this to happen.
- η is free parameter $\rightarrow$ choose it favourable: -0.01.
- This guarantees top-flavoured DM (see direct detection section for motivation).
- Constraint cuts out valid area for $D_{\lambda,ii}$ depending on m_ϕ and m_χ.
- Lower bound on m_χ due to upper limits for $D_{\lambda,ii}$, depending on m_ϕ.

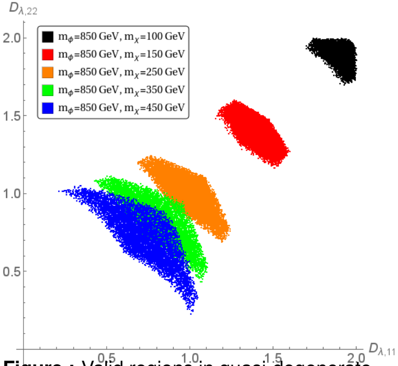

Figure : Valid regions in quasi-degenerate freeze-out scenario.

Single Flavour Freeze-Out (SFF) Szenario

- Only m_χ present at freeze-out.
- We require the mass splitting to be more than 10% (significantly bigger than T_f) for this to happen.
- η is free parameter $\rightarrow$ choose it favourable: -0.075.
- This guarantees top-flavoured DM (see direct detection section for motivation).
- Constraint cuts out valid area of parameters depending on m_ϕ and m_χ, with significant effect on mixing angles.
- In addition to lower bound, we also find an upper bound on m_χ due to upper and lower (from mass splitting condition) limits for $D_{\lambda,ii}$, depending on m_ϕ.

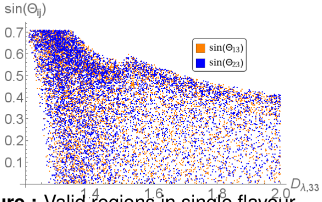

Figure : Valid regions in single flavour freeze-out scenario for $m_\phi = 850$ GeV and $m_\chi = 210$ GeV.

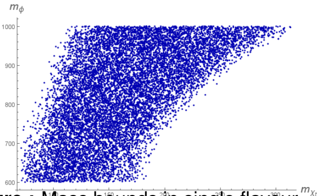

Figure : Mass bounds in single flavour freeze-out scenario.

DM Bounds from Direct Detection Experiments

Many contributions to total WIMP-nucleon cross section:

$$\sigma_n^{SI} = \frac{\mu_n^2}{\pi A^2}|Zf_p + (A-Z)f_n|^2.$$

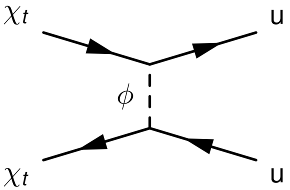

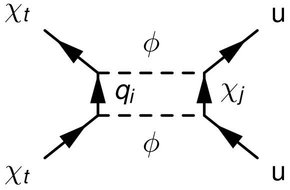

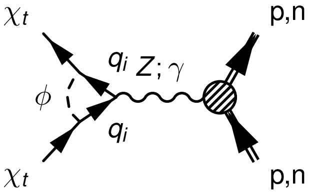

DM Bounds from Direct Detection Experiments

$$f_p^{tree} = 2 f_n^{tree} = \frac{|\lambda_{ut}|^2}{4 m_\phi^2}.$$

$$f_p^{box} = 2 f_n^{box} = \sum_{i,j} \frac{|\lambda_{ui}|^2 |\lambda_{jt}|^2}{32\pi^2 m_\phi^2} F\left(\frac{m_{q_i}^2}{m_\phi^2}, \frac{m_{\chi_j}^2}{m_\phi^2}\right).$$

$$f_p^{photon} = -\sum_i \frac{|\lambda_{it}|^2 e^2}{48\pi^2 m_\phi^2} \left(\frac{3}{2} + log\left(\frac{m_{q_i}^2}{m_\phi^2}\right)\right).$$

$$f_p^Z = -\sum_i \frac{3|\lambda_{it}|^2 e^2 \left(\frac{1}{2} - 2sin^2(\Theta_W)\right)}{32\pi^2 sin^2(\Theta_W) cos^2(\Theta_W) m_Z^2} \frac{m_{q_i}^2}{m_\phi^2} \left(1 + log\left(\frac{m_{q_i}^2}{m_\phi^2}\right)\right).$$

$$f_n^Z = -\sum_i \frac{3|\lambda_{it}|^2 e^2 \left(-\frac{1}{2}\right)}{32\pi^2 sin^2(\Theta_W) cos^2(\Theta_W) m_Z^2} \frac{m_{q_i}^2}{m_\phi^2} \left(1 + log\left(\frac{m_{q_i}^2}{m_\phi^2}\right)\right).$$

DM Bounds from Direct Detection Experiments

[LUX collaboration '15]

- All contributions have to combine to a WIMP-nucleon cross-section below the LUX bounds.
- All contributions are positive, only the Z-penguin with the neutron is negative $\Rightarrow$ saves the day.
- Largest contribution comes from tree-level process. Largest negative term is hence interference term of tree-level and neutron Z-penguin.
- Most important terms, have to nearly cancel each other:

$$A_{\mathcal{I}} \cdot D^4_{\lambda,33} \cdot sin(\theta_{13})^4 - A_{\mathcal{II}} \cdot D^4_{\lambda,33} \cdot sin(\theta_{13})^2 \cdot cos(\theta_{13})^2 \cdot cos(\theta_{23})^2$$

Figure : Cancellation of tree-level and neutron Z-penguin contributions (symbolic).

DM Bounds from Direct Detection Experiments

- Tree level and neutron Z-penguin have to nearly cancel each other.
  $\Rightarrow$ serious constraints on θ_{13}
- For higher couplings the cancellation gets more complicated.
- For too large couplings the cancellation is no longer possible at all
  $\rightarrow$ excluded.
- Top-flavoured DM is the natural choice:
  $\Rightarrow$ Tree-level contribution small
  $\Rightarrow$ Neutron Z-penguin contribution large.

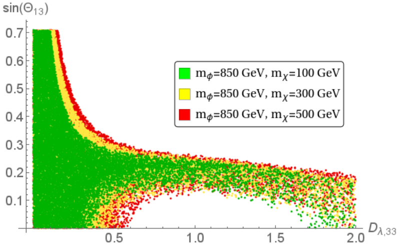

Figure : Valid mixing angle Θ_{13} vs $D_{\lambda,33}$.

Combined Analysis of Constraints (QDF)

Combined application of both flavour, relic abundance and direct detection constraint in quasi-degenerate freeze-out scenario.

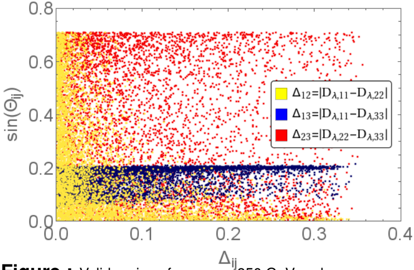

Figure : Valid regions for m_ϕ = 850 GeV and m_χ = 150 GeV (QDF).

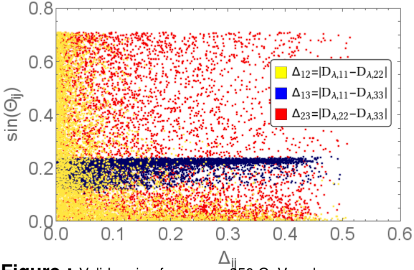

Figure : Valid region for m_ϕ = 850 GeV and m_χ = 250 GeV (QDF).

Combined Analysis of Constraints (QDF)

- A combination of relic abundance and direct detection constraints confine θ_{13} to a narrow interval.
- The bounds on the DM mass become more serious, since the parameters do not only have to fulfill relic abundance constraints.
- The combined analysis clearly prefers top-flavoured DM.

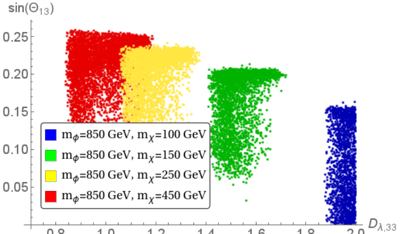

Figure : Valid regions in θ_{13}-$D_{\lambda,33}$-plane (QDF).

Combined Analysis of Constraints (SFF)

Combined application of both flavour, relic abundance and direct detection constraint in single flavour freeze-out scenario.

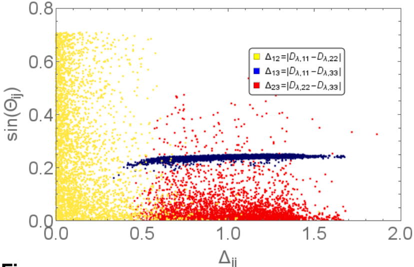

Figure : Valid region for $m_\phi = 850$ GeV and $m_\chi = 225$ GeV (SFF).

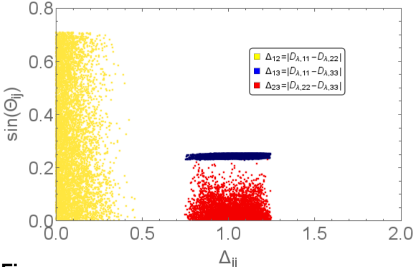

Figure : Valid regions for $m_\phi = 850$ GeV and $m_\chi = 250$ GeV (SFF).

Combined Analysis of Constraints (SFF)

- A combination of relic abundance and direct detection constraints confine θ_{13} to a narrow interval (even more serious than in QDF).
- Especially in SFF the combination of all constraints extremely limits the chance of finding a valid configuration of all parameters for $m_{\chi_t} \leq m_{top}$.
- The combined analysis clearly prefers top-flavoured DM.

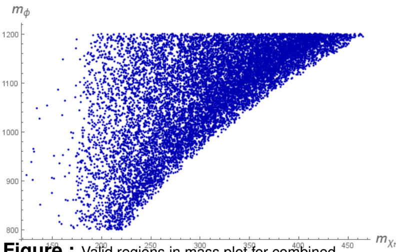

Figure : Valid regions in mass plot for combined constraints (SFF).

Backup Material 1

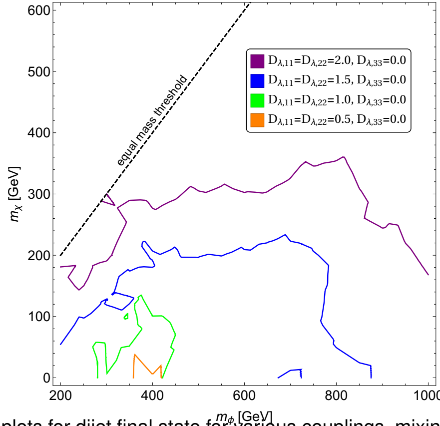

Figure : Exclusion plots for dijet final state for various couplings, mixing angles set to zero.

Backup Material 2

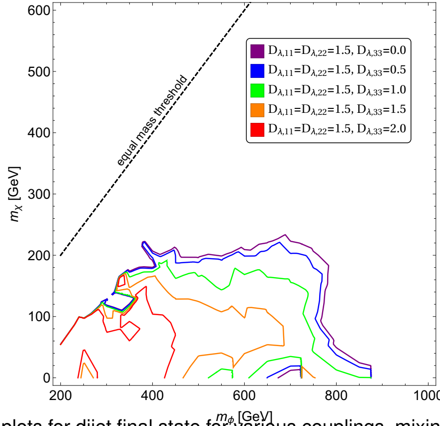

Figure : Exclusion plots for dijet final state for various couplings, mixing angles set to zero.

Backup Material 3

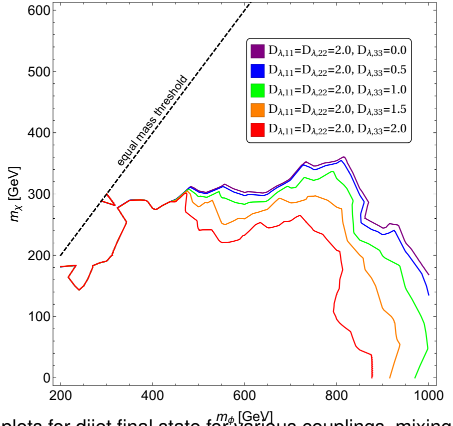

Figure : Exclusion plots for dijet final state for various couplings, mixing angles set to zero.

Backup Material 4

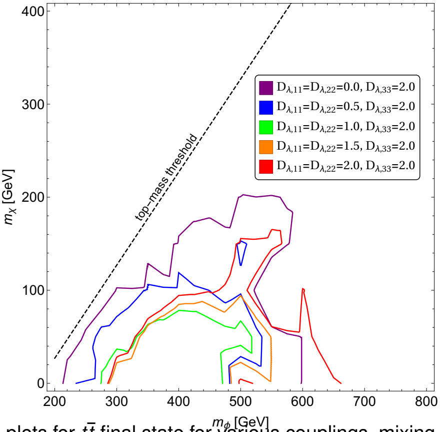

Figure : Exclusion plots for $t\bar{t}$ final state for various couplings, mixing angles set to zero.

Backup Material 5a

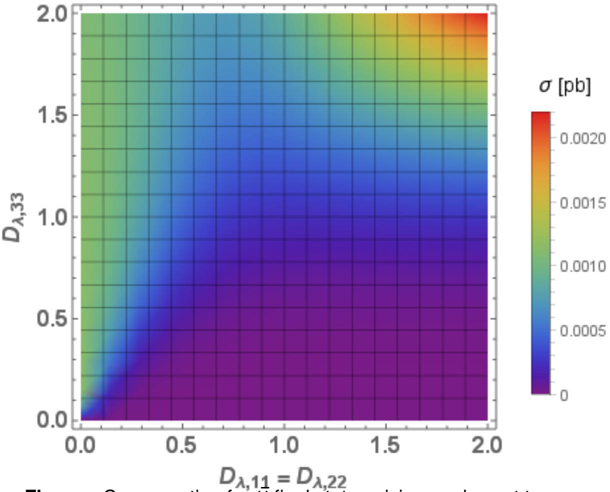

Figure : Cross section for $t\bar{t}$ final state, mixing angles set to zero.

References

Backup Material 5b

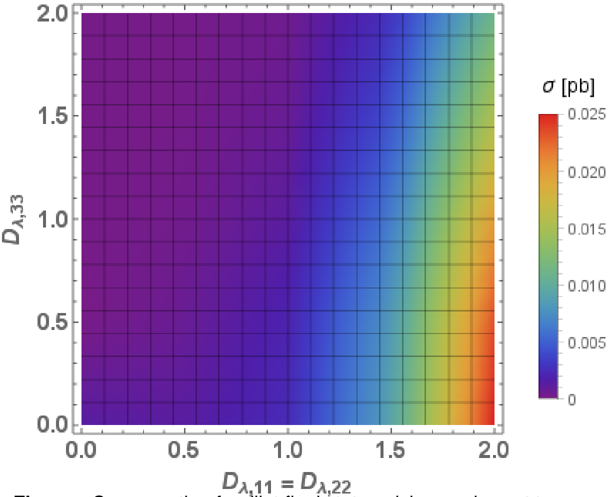

Figure : Cross section for dijet final state, mixing angles set to zero.

References

Backup Material 6

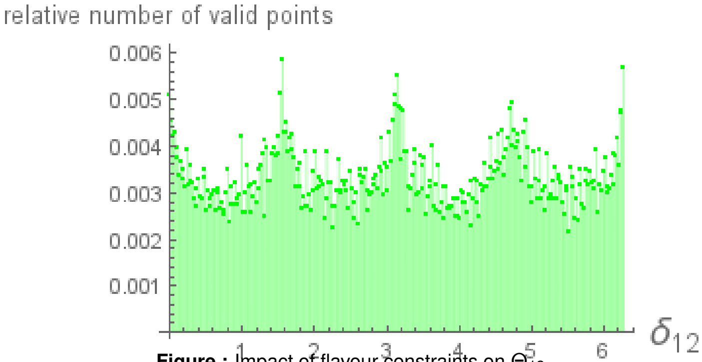

Figure : Impact of flavour constraints on Θ_{12}.

Backup Material 7

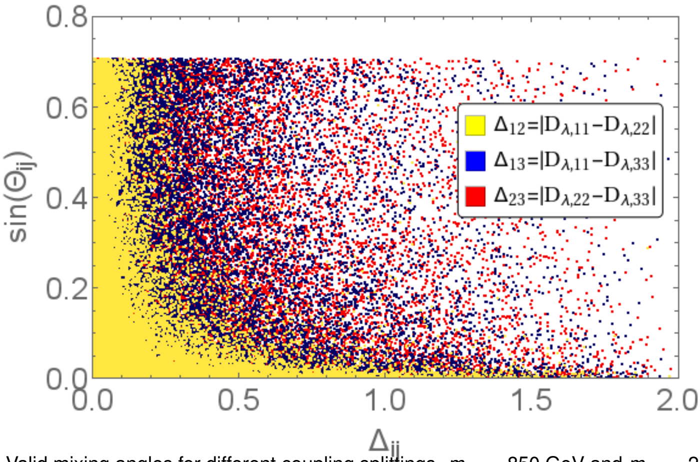

Figure : Valid mixing angles for different coupling splittings. $m_\phi = 850$ GeV and $m_\chi = 250$ GeV.

Backup Material 8

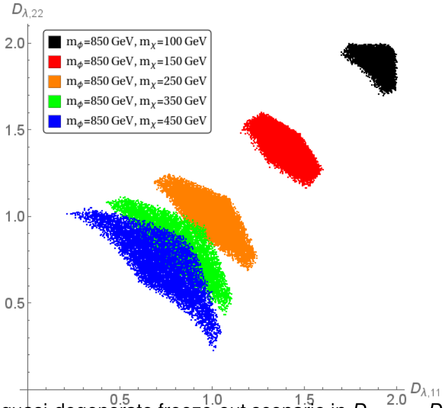

Figure : Valid regions in quasi-degenerate freeze-out scenario in $D_{\lambda,11} - D_{\lambda,22}$-plane for various DM masses.

Backup Material 9

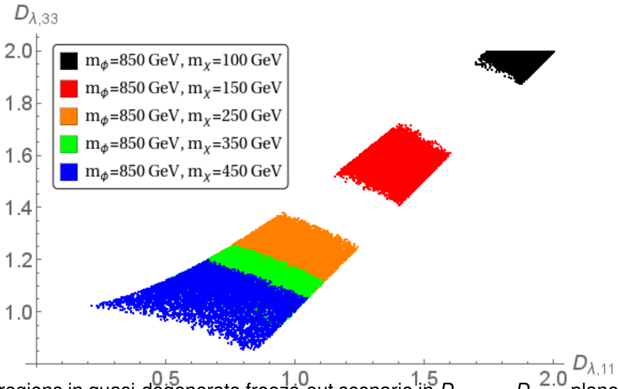

Figure : Valid regions in quasi-degenerate freeze-out scenario in $D_{\lambda,11} - D_{\lambda,33}$-plane for various DM masses.

Backup Material 10

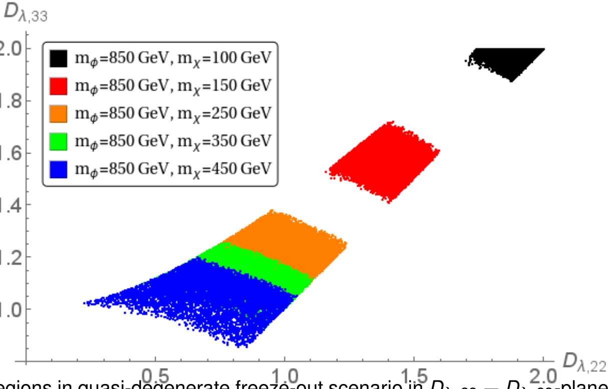

Figure : Valid regions in quasi-degenerate freeze-out scenario in $D_{\lambda,22} - D_{\lambda,33}$-plane for various DM masses.

Backup Material 11

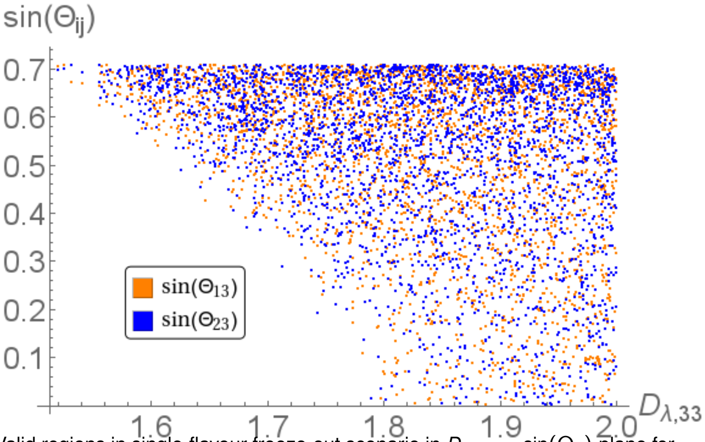

Figure : Valid regions in single-flavour freeze-out scenario in $D_{\lambda,33} - \sin(\Theta_{ij})$-plane for $m_\phi = 850$ GeV and $m_\chi = 150$ GeV.

Backup Material 12

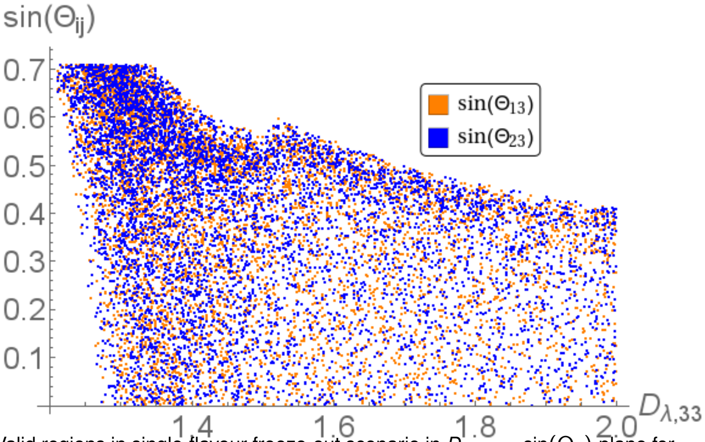

Figure : Valid regions in single-flavour freeze-out scenario in $D_{\lambda,33} - \sin(\Theta_{ij})$-plane for $m_\phi = 850$ GeV and $m_\chi = 210$ GeV.

Backup Material 13

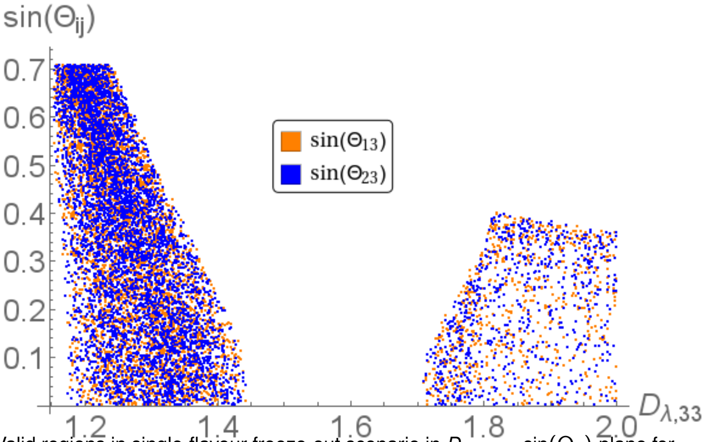

Figure : Valid regions in single-flavour freeze-out scenario in $D_{\lambda,33} - \sin(\Theta_{ij})$-plane for $m_\phi = 850$ GeV and $m_\chi = 230$ GeV.

Backup Material 14

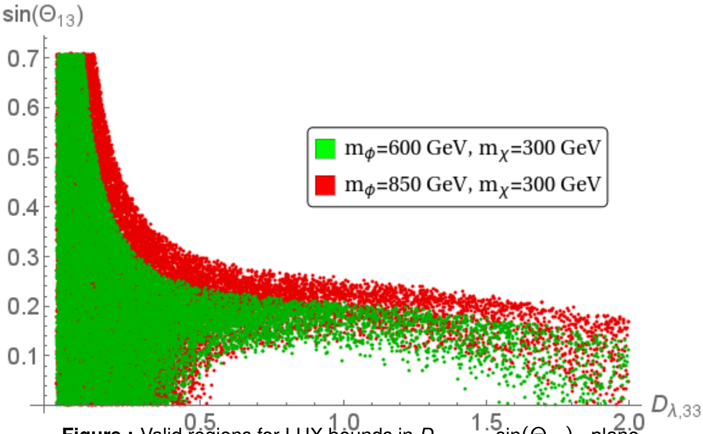

Figure : Valid regions for LUX bounds in $D_{\lambda,33} - \sin(\Theta_{13})-$plane.

Backup Material 15

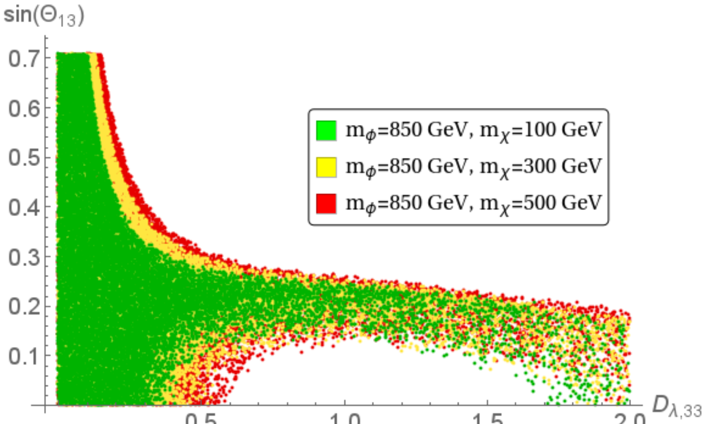

Figure : Valid regions for LUX bounds in $D_{\lambda,33} - \sin(\Theta_{13})$−plane.

Backup Material 16

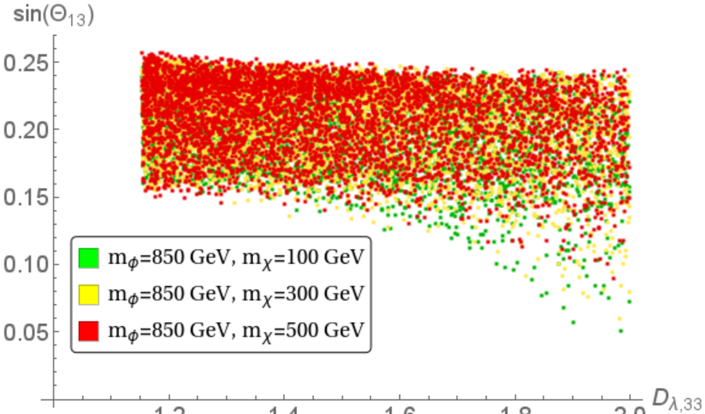

Figure : Valid regions for LUX bounds in $D_{\lambda,33} - \sin(\Theta_{13})-$plane, with SFF splitting applied.

Backup Material 17

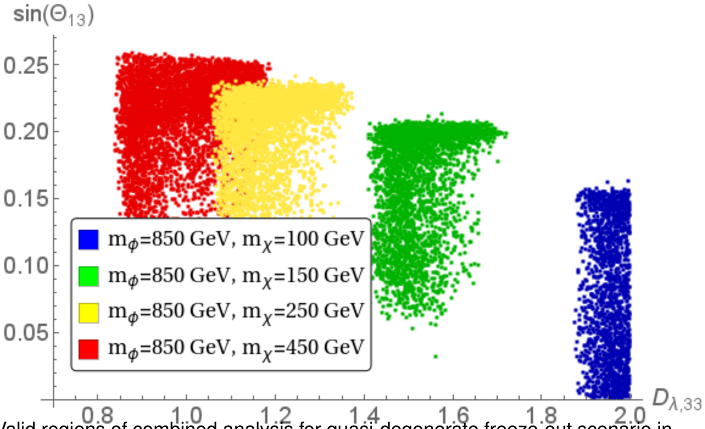

Figure : Valid regions of combined analysis for quasi-degenerate freeze-out scenario in $D_{\lambda,33} - \sin(\Theta_{13})-$plane for different DM masses.

Backup Material 18

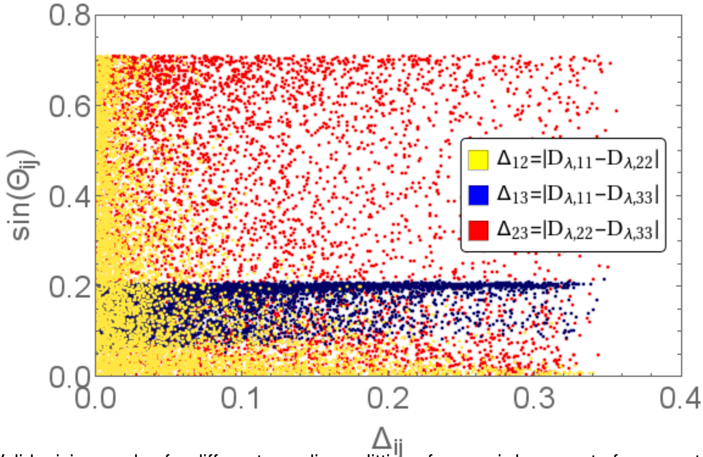

Figure : Valid mixing angles for different coupling splittings for quasi-degenerate freeze-out scenario. $m_\phi = 850$ GeV and $m_\chi = 150$ GeV.

Backup Material 19

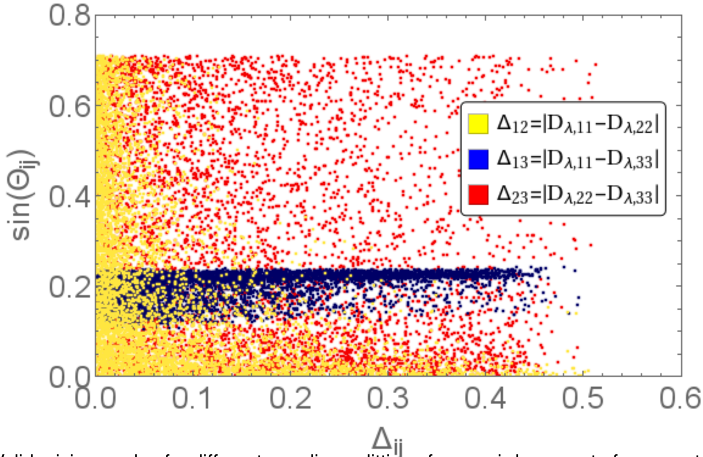

Figure : Valid mixing angles for different coupling splittings for quasi-degenerate freeze-out scenario. $m_\phi = 850$ GeV and $m_\chi = 250$ GeV.

Backup Material 20

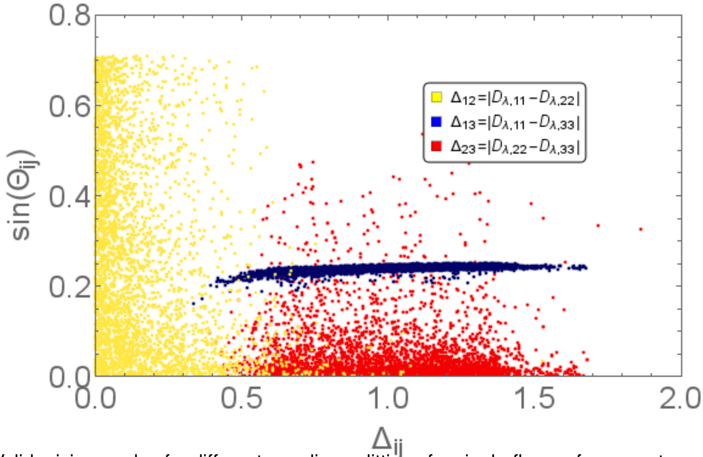

Figure : Valid mixing angles for different coupling splittings for single-flavour freeze-out scenario. $m_\phi = 850$ GeV and $m_\chi = 225$ GeV.

Backup Material 21

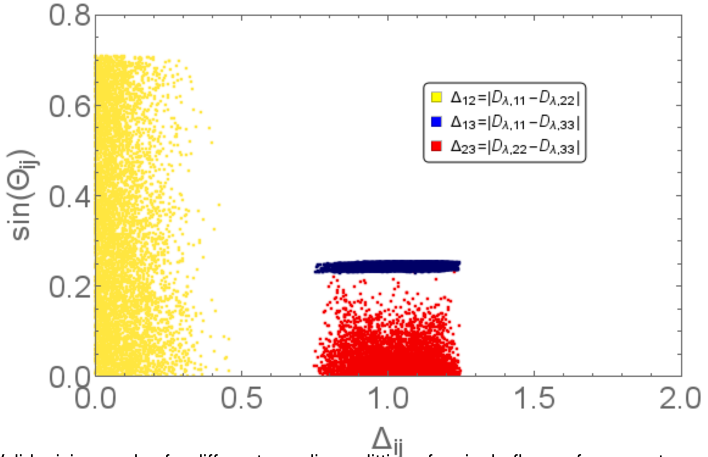

Figure : Valid mixing angles for different coupling splittings for single-flavour freeze-out scenario. $m_\phi = 850$ GeV and $m_\chi = 250$ GeV.

Backup Material 22

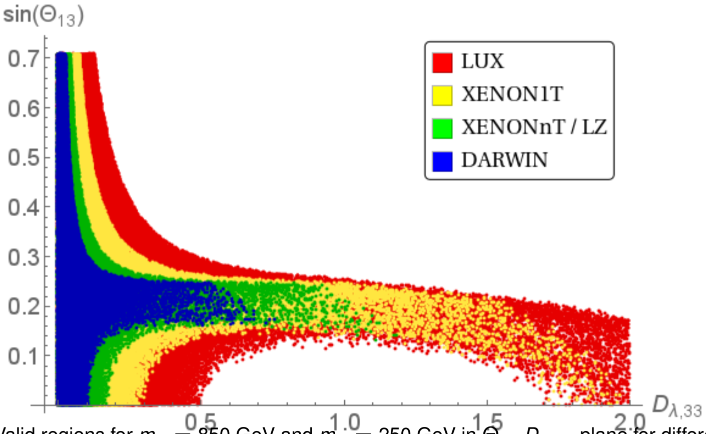

Figure : Valid regions for $m_\phi = 850$ GeV and $m_\chi = 250$ GeV in Θ_{13}-$D_{\lambda,33}$-plane for different strengths of direct detection constraints in QDF.

Backup Material 23

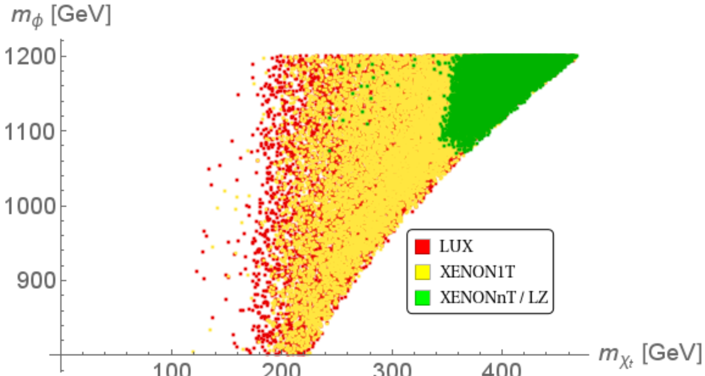

Figure : Valid regions in Mass Scan for different strengths of direct detection constraints in SFF.

Backup Material 24

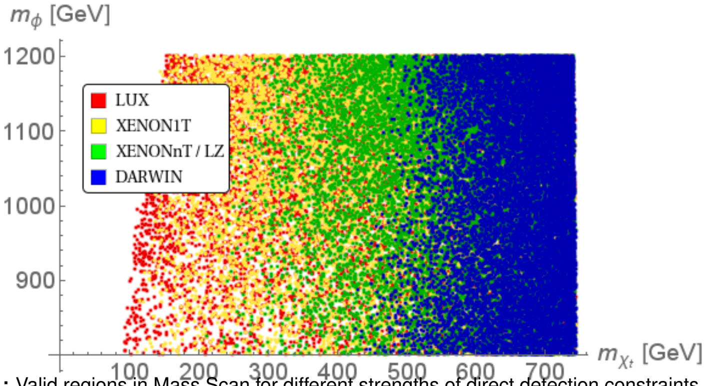

Figure : Valid regions in Mass Scan for different strengths of direct detection constraints in QDF.